EJN European Journal of Neuroscience

FENS Federation of European Neuroscience Societies

European Journal of Neuroscience, Vol. 41, pp. 586–602, 2015 doi:10.1111/ejn.12811

Sensorimotor neural dynamics during isochronous tapping in the medial premotor cortex of the macaque

Hugo Merchant, Oswaldo Pérez, Ramón Bartolo, Juan Carlos Méndez, Germán Mendoza, Jorge Gámez, Karyna Yc and Luis Prado

Instituto de Neurobiología, UNAM, Campus Juriquilla, Boulevard Juriquilla No. 3001, Querétaro, Qro. 76230, México

Keywords: medial premotor areas, rhesus monkeys, sensorimotor integration, timing mechanism

Abstract

We determined the response properties of neurons in the primate medial premotor cortex that were classified as sensory or motor during isochronous tapping to a visual or auditory metronome, using different target intervals and three sequential elements in the task. The cell classification was based on a warping transformation, which determined whether the cell activity was statistically aligned to sensory or motor events, finding a large proportion of cells classified as sensory or motor. Two distinctive clusters of sensory cells were observed, i.e. one cell population with short response-onset latencies to the previous stimulus, and another that was probably predicting the occurrence of the next stimuli. These cells were called sensory-driven and stimulus-predicting neurons, respectively. Sensory-driven neurons showed a clear bias towards the visual modality and were more responsive to the first stimulus, with a decrease in activity for the following sequential elements of the metronome. In contrast, stimulus-predicting neurons were bimodal and showed similar response profiles across serial-order elements. Motor cells showed a consecutive activity onset across discrete neural ensembles, generating a rapid succession of activation patterns between the two taps defining a produced interval. The cyclical configuration in activation profiles engaged more motor cells as the serial-order elements progressed across the task, and the rate of cell recruitment over time decreased as a function of the target interval. Our findings support the idea that motor cells were responsible for the rhythmic progression of taps in the task, gaining more importance as the trial advanced, while, simultaneously, the sensory-driven cells lost their functional impact.

Introduction

The quantification of the passage of time in the hundreds of milliseconds is a critical element for complex behaviors such as the performance of sports (Merchant & Georgopoulos, 2006; Merchant *et al.*, 2009), and the execution and appreciation of music (Janata & Grafton, 2003; Phillips-Silver & Trainor, 2005). Humans have the ability to quantify intervals, defined by different sensory modalities, in a variety of perceptual or motor activities (Merchant *et al.*, 2013a). Remarkably, the temporal precision increases as a function of the number of timed intervals in a sequence (Ivry & Hazeltine, 1995; Grondin, 2001; Merchant *et al.*, 2008a). This is particularly true during the execution of isochronous taps, where the interval-timing mechanism benefits from the predictive rhythmic structure of the cyclical behavior (Merchant *et al.*, 2008b). A large amount of evidence supports the existence of a partially distributed timing mechanism, integrated by core structures such as the motor cortico-thalamic-basal ganglia circuit, and areas that are selectively engaged by different behavioral contexts (Buhusi & Meck, 2005; Coull *et al.*, 2011; Merchant *et al.*, 2011a; Stauffer *et al.*, 2012; Merchant *et al.*, 2013a). For example, neurophysiological experiments in behaving monkeys have shown that neurons in the medial premotor cortex (MPC) (pre-supplementary motor area and supplementary motor area proper) are tuned to the duration of intervals during isochronic tapping (Merchant *et al.*, 2013b; Bartolo *et al.*, 2014). Thus, the fact that a subgroup of these interval-tuned neurons showed similar preferred intervals across modalities and during tasks involving the production of one or multiple intervals corroborates the hypothesis that the MPC is part of the core timing mechanism. Furthermore, a gain mechanism for the encoding of the total number of produced intervals in a sequence has been documented, where the discharge rate for the preferred interval of tuned cells increases for larger numbers of produced intervals (Merchant *et al.*, 2013b). Accordingly, functional imaging studies in humans showed that the execution of complex rhythmic sequences produces higher activity in the MPC than isochronous movements (Dhamala *et al.*, 2003; Bengtsson *et al.*, 2005).

The synchronisation-continuation task (SCT) has been a pivotal paradigm in the study of time production. In this task, subjects synchronise taps with pacing isochronous brief stimuli and then continue tapping at the instructed rate without the advantage of the sensory metronome (Wing, 2002). In order to synchronise their responses in the initial part of this task, subjects not only need to attend to the pacing stimuli and generate a predicted sequence of sensory events, but also to produce a predictive tapping behavior with a particular temporal and sequential structure. This phase of the task also requires the recognition and correction of errors between the incoming and predicted sensory events and the actual tapping sequence (Lewis *et al.*, 2004). The neural substrate of these

Correspondence: Dr Hugo Merchant, as above.
E-mail: hugomerchant@unam.mx

Received 25 August 2014, accepted 26 November 2014

processes is unknown. Therefore, the present article provides the first neurophysiological evidence in the MPC regarding the dynamic processing of sensory signals, sensorimotor transformations, and motor commands during isochronous tapping to a sensory metronome.

Materials and methods

General

All of the animal care, housing, and experimental procedures were approved by the National University of Mexico Institutional Animal Care and Use Committee and conformed to the principles outlined in the Guide for Care and Use of Laboratory Animals (NIH, publication number 85-23, revised 1985). The two monkeys (*Macaca mulatta*, both males, 5–7 kg body weight) were monitored daily by the researchers and the animal care staff to check their conditions of health and welfare.

Synchronisation-continuation task

The SCT has been described in detail previously (Zarco *et al.*, 2009; Merchant *et al.*, 2011a). Briefly, on each trial the monkey tapped a button seven times in succession, with the goal of maintaining a constant inter-tap interval across all taps. The first four taps were made synchronously with a repetitive cue stimulus (either a visual stimulus presented on a computer monitor or an auditory tone via speakers). The monkey then had to tap the button three more times with the same inter-tap duration but without sensory guidance (continuation phase) (Fig. 1A). Hence, this task had six serial-order elements, three in the synchronisation phase and three in the continuation phase. Five different target intervals were used: 450, 550, 650, 850, and 1000 ms. During the recording of each group of cells (one 'set'), the monkey performed five repetitions of each target interval (for a total of 25 trials), with durations randomly ordered within each repetition. Trials were separated by an inter-trial interval of 1.2–4 s.

Neural recordings

The extracellular activity of single neurons in the medial premotor areas was recorded using a system with seven independently movable microelectrodes (Merchant *et al.*, 2001) (1–3 MΩ, Uwe Thomas Recording, Germany). All of the isolated neurons were recorded regardless of their activity during the task, and the recording sites changed from session to session. At each site, raw extracellular membrane potentials were sampled at 40 kHz. Single-unit activity was extracted from these records using an off-line sorter (Plexon, Dallas, TX, USA). Structural magnetic resonance imaging (MRI) was used to localise the recording sites (Merchant *et al.*, 2011a). An initial ANOVA using the discharge rate during the key holding (control) period as dependent variable, and the recording time across all trials of the SCT as a factor was performed for each neuron to identify cells whose activity changed significantly during the recording. A significant variation of the baseline rate across trials was taken to indicate instability of the cell's task responsiveness, and therefore these cells were excluded from further analyses. It is important to clarify that the 1083 cell database used in the present article has

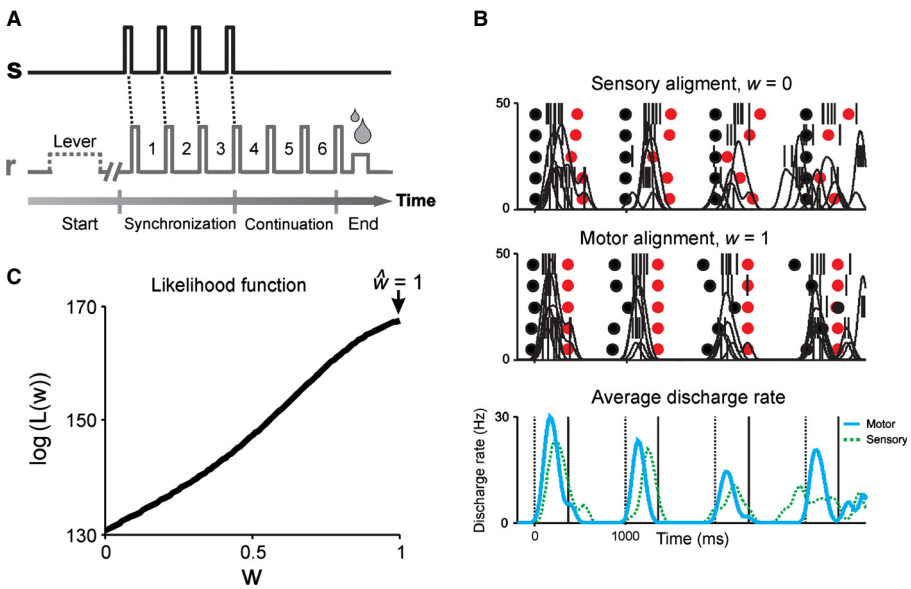

FIG. 1. Task and time-warping analysis. (A) The SCT. Monkeys were required to push a button (r, gray line) each time that stimuli with a constant inter-stimulus target interval (s, black line) were presented, which resulted in a stimulus–movement cycle. After four consecutive synchronised movements, the stimuli stopped, and the monkeys continued tapping with a similar target interval for three additional intervals. Hence, six inter-tap intervals were generated by the monkeys in each trial. The instructed durations, defined by brief auditory or visual stimuli, were 450, 550, 650, 850, and 1000 ms, and were chosen pseudo-randomly within a repetition. (B) The cell activity during the synchronisation of the SCT was used to determine whether the activity of the cell was better aligned to sensory or motor events using the time-warping analysis. Simulated spike trains of a motor cell during the synchronisation phase of the SCT are shown. Top: Raster plot of the simulated activity aligned to the stimulus presentations (black circles) with an inter-stimulus interval of 1000 ms, where every tick mark corresponds to a single spike time stamp and the spike density functions for each trial are shown as a black line. Middle: The same responses as shown at the top, but aligned to the button press (red circles) using the transformation in eqn 1. Bottom: The average spike density function (eqn 3) is shown for the sensory (continuous blue line) or motor (dotted green line) alignments. The black vertical dotted lines correspond to the stimulus time events, whereas the vertical continuous lines correspond to the warping motor events. (C) The logarithm of the homogeneity measure log($L(w)$), computed from eqn 5, is plotted as a function of the warping value. The larger warping value ($\hat{w}$) is equal to 1.

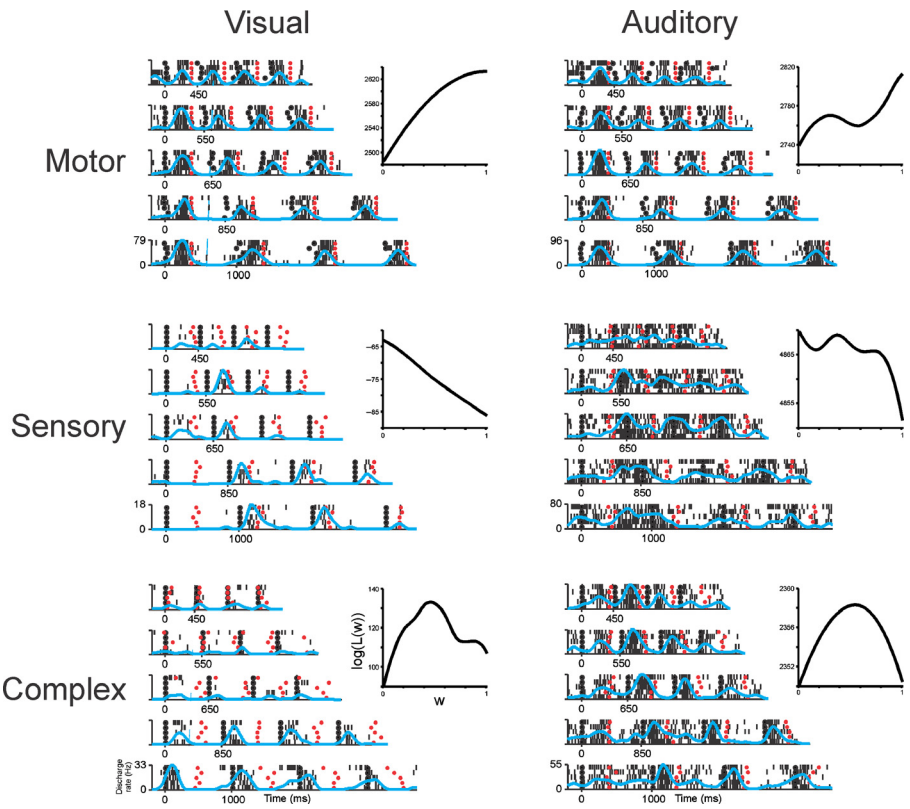

FIG. 2. The raster plots of the activity of cells classified in the time-warping analysis as motor (top), sensory (middle), or complex (bottom) for the visual and auditory conditions. Every tick mark corresponds to a single spike time stamp in a correct trial. The spike density function averages (blue line) are below each raster. The black circles represent the stimulus presentation and the red circles represent the button press. The five target intervals are shown. Motor cells are aligned to the button press, whereas sensory and complex cells are aligned to the stimuli. The insets show the logarithm of homogeneity measure log ($L(w)$) as a function of w. For each neuron, the larger warping value ($\hat{w}$) is equal to 1 for the motor, equal to 0 in the sensory, and close to 0.5 in the complex cells.

been analysed previously in other conceptual contexts (Merchant *et al.*, 2011a, 2013b).

Identification of recording locations

We determined the position of the recording sites relative to the brain sulci using structural MRI. Custom-made plastic tubes filled with an aqueous solution of vitamin E ran through the perimeter and center of the recording chamber and were employed as fiducial objects to localise the recording chamber relative to the anatomical landmarks in an MRI volume. Monkeys were sedated throughout the image-acquisition procedure using a mixture of ketamine (10 mg/kg) and xylazine (0.25 mg/kg), and placed in an MRI-compatible stereotaxic apparatus. The scan parameters were as follows: a high-resolution T1-weighted gradient echo sequence was acquired [repetition time (TR), 20 ms; echo time (TE), 6.9 ms; flip angle, 25°; matrix, 240 × 108; slices, 80; resolution, 1.0 × 1.0 × 1.0 mm; coronal slices, acquisition time, 5 min 24 s] with a 1.0 T Philips Intera MRI Scanner. Images were transferred to a workstation in the laboratory for further analysis using MRICRO[2] (Rorden *et al.*, 2007) and IMAGEJ (http://rsbweb.nih.gov/ij/; developed by Wayne Rasband, National Institutes of Health, Bethesda, MD, USA).

Once we identified the center of the recording chamber for the two monkeys in relation to the brain sulci, we placed the approximate recording locations inside the chamber, based on the location description for each recording penetration from our experimental protocols. Hence, considering this last point and the fact that the functional MRI resolution was 1 mm, it is important to emphasise that the reported recording locations (depicted in Fig. 3) are only approximations of the real recording locations.

Data analysis

Selection of significant cells

We selected for further analysis those cells whose firing rates were significantly related to either the serial order or target interval, using a two-way ANOVA that included as factors the serial order, target interval, and serial order × target interval interaction. Cells were included if their activity was significantly related to the serial order and/or target interval in this ANOVA at a threshold of $P < 0.05$. Of the 1083 cells, 607 and 540 cells met this inclusion criterion for the visual and auditory conditions, respectively, and were used in the subsequent analyses. It is important to emphasise that all of the analyses were carried out only during the synchronisation phase of the SCT.

Identification of sensory and motor neurons – time-warping analysis

We previously proposed a warping transformation (Perez *et al.*, 2013) to determine whether the activity of a cell was better aligned to sensory or motor events during the synchronisation phase of the SCT. We defined the time of sensory events as the instant in which

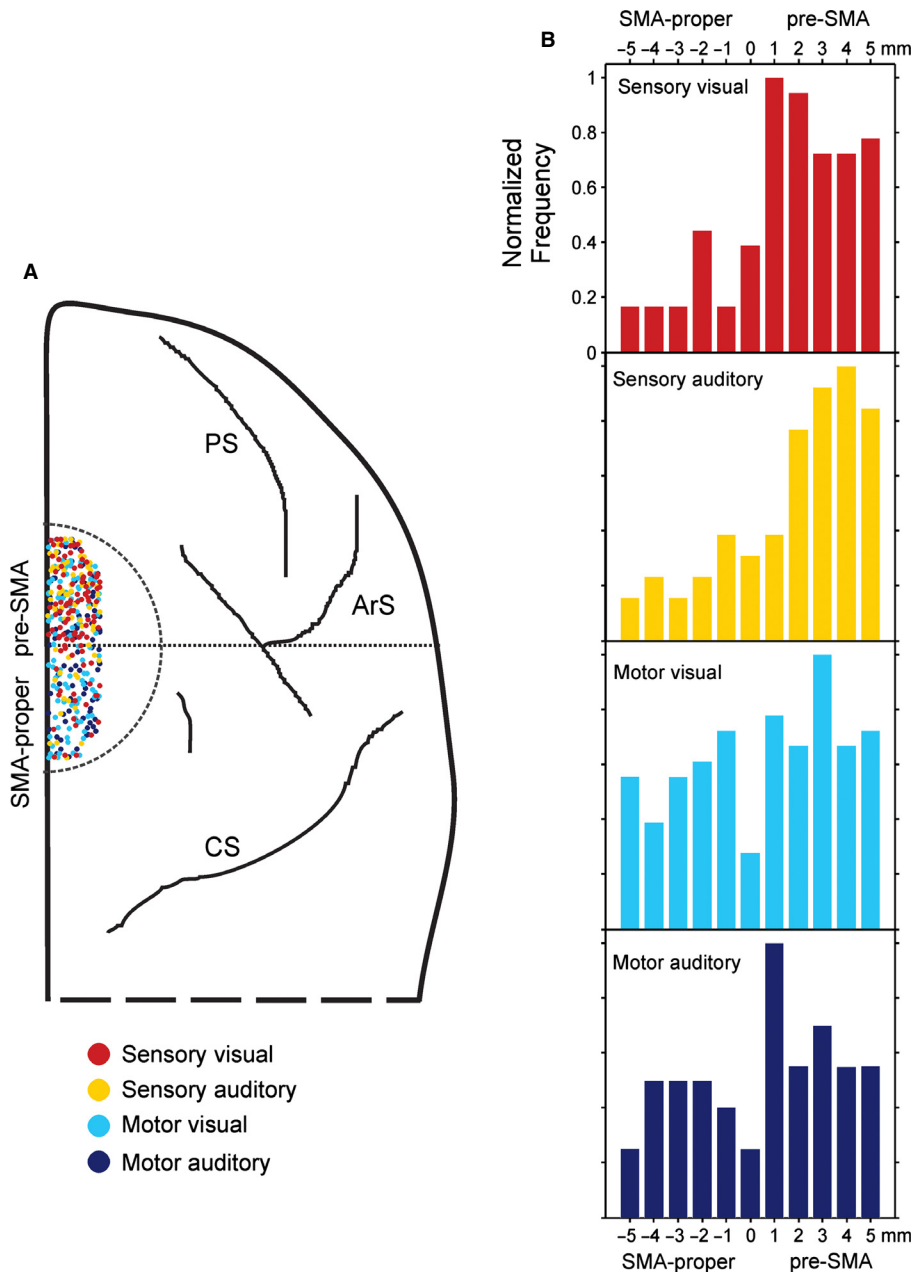

FIG. 3. Top view of the medial premotor areas and the location of different cell types. (A) MRI surface reconstruction of macaque brain and recording sites in the two monkeys. Colored dots correspond to the cell types as in the key below. PS, principal sulcus; ArS, arcuate sulcus; CS, central sulcus; surface bounded by a semicircle, recording area and MPC. The line dividing the circle corresponds to the hypothetical division between the SMA proper (caudal) and pre-SMA (rostral). (B) Frequency histograms of the distribution of the different cell types in the two medial premotor areas. The data from the two monkeys were similar and were pooled in this figure.

the auditory or visual stimulus was presented. The time of motor events was defined as the moment in which the monkey tapped on the button. The goal of this analysis was to find the cell alignment that produced the smallest inter-trial variability (Fig. 1B). The method had the following steps:

(1) The action potential times $\{t_{i,j}\}$ were initially aligned to the stimulus times $\{S_{i,1}, S_{i,2}, S_{i,3}, S_{i,4}\}$, where i corresponds to the trial repetition and j to the spike number. In addition, we defined the following transformation in order to align the action potential times $\{t_{i,j}\}$ to the motor events $\{M_{i,1}, M_{i,2}, M_{i,3}, M_{i,4}\}$

$$T_i(t) = \frac{L_{j+1} - L_j}{M_{i,j+1} - M_{i,j}}\left(t - M_{i,j}\right) + L_j \qquad (1)$$

when $M_{i,j} \leq t \leq M_{i,j+1}$ and $\{L_1, L_2, L_3, L_4\}$ were landmark references. L_1 was the average reaction time of the monkeys for the first stimulus during cell recordings, whereas L_2 to L_4 were defined as the target intervals (i.e. 450, 550, 650 ms, etc.). This transformation was performed for each trial across the five target intervals in the SCT.

(2) The warping transformation was

$$T_w^i(t) = wT_i(t) + (1-w)t \tag{2}$$

that depended on the parameter w. When $w = 0$ the responses were aligned to the sensory events S. When $w = 1$ the responses were aligned to the motor events M. w values between 0 and 1, in steps of 0.1, produced alignments between S and M events.

(3) The average spike density function $r_w(t)$ for every target interval across trials was computed using the following equation for a particular w.

$$r_w(t) = \frac{1}{N}\sum_{i=1}^{N}\sum_{j=1}^{n_i}\frac{1}{\sqrt{2\pi}\sigma}e^{-\frac{(t-T_w^i(t_{i,j}))^2}{2\sigma^2}} \tag{3}$$

where n_i is the total number of action potentials in a trial i, N is the total number of trials, and the Gaussian kernel width σ =20 ms.

(4) The likelihood function representing the multi-trial response variability of a cell, for a particular w alignment, was calculated assuming that $D_i = \{t_{i,1}, t_{i,2}, \ldots, t_{i,n_i}\}$, the times of n_i spikes in trial i, is a non-homogeneous Poisson process with rate $r_w(t)$

$$L_i(w) = p(D_i|w) = e^{-\int_0^T r_w(t)dt}\prod_{j=1}^{n_i} r_w\left(t_{i,j}\right) \tag{4}$$

As the likelihood function represents the multi-trial response variability of a cell using the average spike density function, we used a leave-one-out cross-validation method to determine the variability of trial i from the average firing rate. Then, for every neuron, we computed the total probability that was the product of $L_i(w)$ for every trial i and for each of the five target intervals *Int*

$$L(w) = \prod_{Int}\prod_{i} L_i(w) \tag{5}$$

Finally, we found the w that maximised the function $L(w)$, which corresponds to the value that maximises the spike prediction accuracy across trials and was called the warping value ($\hat{w}$) (see Fig. 1C). Consequently, this measure is associated with the warping value that minimises the inter-trial variability of the cell activity.

Bayes factors

The warping transformation finds the best-fitting alignment of a cell. However, it is important to determine the probability of assigning a particular warping value to a sensory or motor alignment. Let D be the set of all spike times of a neuron across trials and target intervals. For cell i we have

$$\begin{aligned} p(D|sensory) &= L(0) \\ p(D|motor) &= L(1) \\ p(D|complex) &= \int_0^1 L(w)dw \end{aligned} \tag{6}$$

We then define the following Bayes factors

$$\gamma_1 = log_{10}\left(\frac{p(D|motor)}{p(D|sensory)}\right)$$

$$\gamma_2 = log_{10}\left(\frac{p(D|motor)}{p(D|complex)}\right)$$

$$\gamma_3 = log_{10}\left(\frac{p(D|sensory)}{p(D|complex)}\right) \tag{7}$$

These factors summarise the evidence provided by the data in favor of one category, i.e. motor (if $\gamma_1 > 0$ and $\gamma_2 > 0$), sensory (if $\gamma_1 < 0$ and $\gamma_3 > 0$), and complex (if $\gamma_2 < 0$ and $\gamma_3 < 0$). We classified the cells in three different categories based on this information as follows: motor neuron if $\gamma_1 > 1$ and $\gamma_2 > 1$, sensory neuron if $\gamma_1 < -1$ and $\gamma_3 > 1$, and complex neuron if $\gamma_2 < -1$ and $\gamma_3 < -1$. Cells that did not meet any of the criteria for classification were considered indeterminate. Therefore, the γ thresholds used in the present article (a value larger than 1) provide strong evidence in favor of a particular cell category, according to Kass & Raftery (1995). The warping analysis was performed independently for the cell recordings in the auditory and visual SCT conditions.

Identification of cell activation periods – Poisson-train analysis

For the cells classified as sensory or motor by the time-warping analysis, we used the Poisson-train analysis (Hanes *et al.*, 1995) to identify the periods of cell activation within each interval defined by two subsequent stimuli (sensory cells) or two subsequent taps (motor cells). This analysis determines how improbable it is that the number of action potentials within a specific condition (i.e. target interval and ordinal sequence) was a chance occurrence. For this purpose, the actual number of spikes within a time window was compared with the number of spikes predicted by the Poisson distribution derived from the mean discharge rate during the entire recording of the cell. The measure of improbability was the surprise index (*SI*) defined as

$$SI = -logP \tag{8}$$

where P was defined by the Poisson equation

$$P = e^{-rT}\sum_{i=n}^{\infty}\frac{(rT)^i}{i!} \tag{9}$$

and where P is the probability that, given the average discharge rate r, a spike train of a produced interval T contains n or more spikes in a trial. Thus, a large *SI* indicates a low probability that a specific elevation in activity was a chance occurrence (Merchant *et al.*, 2001). This analysis assumes that an activation period is statistically different from the average discharge rate r, considering that the firing of the cell is following a non-homogenous Poisson process (see also Perez *et al.*, 2013).

The spike-train analysis was applied grouping all trials of the three intervals of the synchronisation phase in the SCT (15 intervals, five duration × three intervals in the sequence). We used the algorithm (Hanes *et al.*, 1995) to detect activations above randomness, as described previously (Merchant *et al.*, 2001, 2013b). Briefly, the mean discharge rate (r) was computed for the entire recording session of the cell (i.e. the SCT in the auditory and visual conditions). The first two consecutive spikes that had a mean discharge rate greater than or equal to r were found, and the time between these two spikes was defined as the initial T value. The next spike was then identified and the inter-spike interval between this and the previous spike was added to T. The corresponding *SI* was calculated. This was repeated until the end of the spike train and the spike at the end of the interval T with the maximum *SI* was defined as the end of the burst. Next, the *SI* was calculated for the interval T from

the last to the first spike. The spikes from the beginning were then removed until the end of the spike train, computing the corresponding *SI* in each step. The spike at which *SI* was maximised was defined as the beginning of the burst. All produced intervals that showed a burst larger than 80 ms and an *SI* $P < 0.01$ were considered as having a significant activation. If this criterion was not fulfilled, it was assumed that there was no response for that target duration/ordinal sequence combination. Consequently, the Poisson-train analysis provides the response-onset latency and the extent of the activation period for each cell in a particular combination of target interval/serial order.

Normal distribution analysis

The time-varying changes in activation periods identified with the Poisson-train analysis showed a clear progressive pattern of responses in the motor cell population, where groups of neurons formed functional ensembles that encode information of the SCT during small time windows. The sequential patterns of activation of different neural ensembles showed different dynamics, with distinct rates of cell activation profiles across target intervals and serial order. Hence, we characterised the overall population change in activity as a function of time using an elliptical bivariate normal distribution illustrated in Fig. 9A and B. In this figure, the ellipse is centered at the *x*–*y* mean, where *x* is time aligned to the button press, and *y* is the order of the cells' activation. The activation order was computed by sorting (from minimum to maximum) the mean onset latency (across duration and serial order) of all of the cells with activation periods in the Poisson-train analysis. The lengths of the ellipse axes are proportional to the square root of the two eigenvalues of the *x*–*y* variance–covariance matrix. The two axes are orthogonal, and are equivalent to the variances along each axis (i.e. the larger axis corresponds to the axis of larger variance). We scaled the axis using the constant $x_p^2(\alpha)$, which corresponds to the upper (100α)th percentile of the Chi-squared distribution with *k* degrees of freedom. This leads to an ellipse that contains the $(1 - \alpha) \times 100\%$ of the distribution probability, where $\alpha = 0.8$ (Fig. 9A and B). Finally, the orientation of the ellipse was defined by the angle θ that was equal to the arctangent of the *x* and *y* elements of the eigenvector from the larger eigenvalue (Merchant *et al.*, 2004c). Importantly, this angle determines the rate of information flow in the cell population over time.

Results

Behavioral performance

The activity of MPC neurons was recorded in two monkeys during the performance of a SCT (Fig. 1A), where the animals tapped a button in time with four evenly-spaced visual or auditory stimuli (synchronisation phase) and then continued to tap three more times with same duration (continuation phase). Thus, the task had six serial-order elements, three for each phase. Five instructed inter-tap durations (target intervals) were used: 450, 550, 650, 850, and 1000 ms. Monkeys were able to accurately produce the instructed intervals, showing an average underestimation of ~50 ms across durations in the SCT (Merchant *et al.*, 2013b). The temporal variability of the monkeys' tapping performance (defined as the SD of the individual inter-response intervals) increased linearly as a function of duration. Hence, the monkeys showed appropriate temporal performance in the SCT (Zarco *et al.*, 2009; Merchant & Honing, 2014).

Time-warping analysis – classification of sensory and motor neurons

The main purpose of the present study was to determine the response profiles of cells classified as sensory or motor by the time-warping analysis during the synchronisation phase of the SCT. This phase of the task included a sequence of sensory and motor events. We developed a transformation that allowed us to align spike times to all of the push-button events in a trial (Perez *et al.*, 2013) (see Materials and methods). This transformation depends on a parameter *w* that can acquire values between 0 and 1. When $w = 0$, spikes are completely aligned to the stimuli, as the original data. An example of this alignment is shown for simulated spike trains in Fig. 1B top (black circles). Conversely, when $w = 1$, spike trains are aligned to the motor events, as shown in Fig. 1B middle (red circles). Obviously, when responses were given intermediate *w* values, they were aligned between sensory and motor events, and were considered complex cells. In order to find which *w* value was the best to minimise the inter-trial variability for a given cell, we used a homogeneity measure, *L*, whose value is inversely proportional to this variability. Figure 1B bottom shows that, when the spike times in the top panels are aligned to the motor event, the average spike density functions acquire larger values than when aligned to sensory events, which indicates that the cell responses show less inter-trial variability in the former alignment. In accordance with this, Fig. 1C shows the $log(L(w))$ as a function of *w* for simulated spike trains shown in Fig. 1B, where it can be seen that the highest probability is reached when $\hat{w} = 1$. This means that the best alignment for the activity of this simulated cell was to motor events.

We performed the time-warping analysis in 607 cells in the visual condition and 540 cells in the auditory condition of the SCT. These cells showed significant changes in their activity as a function of the serial order and/or target interval in a two-way ANOVA (see Materials and methods). Representative examples for cells classified by the time-warping analysis as sensory, motor, and complex for the auditory and visual conditions are depicted in Fig. 2.

In addition, $log(L(w))$ as a function of *w* are illustrated in Fig. 2 as an inset in each raster, where motor cells showed the highest probability at $\hat{w} = 1$, sensory cells at $\hat{w} = 0$, and complex cells at $\hat{w} \sim 0.5$. In order to determine how strong was the evidence in the *L* probabilities in favor of one of the response categories illustrated in Fig. 2, we used an additional analytical algorithm called the Bayes factors (γ) (described in eqn 6 and 7). Using the criteria provided by Kass & Raftery (1995) we classified each cell into the three categories using the following γ thresholds: motor when $\gamma_1 > 1$ and $\gamma_2 > 1$, sensory when $\gamma_1 < -1$ and $\gamma_3 > 1$, and complex when $\gamma_2 < -1$ and $\gamma_3 < -1$. Otherwise, the cells were categorised as indeterminate.

The results of the Bayes factors analysis on our database, depicted in Table 1, shows that most of the neurons [309/607 (51%) for the visual and 259/540 [48%] for the auditory condition] recorded in the MPC during the synchronisation phase of the SCT were classified as motor. Nevertheless, a large percentage of cells were also classified as sensory (see Table 1). These findings suggest that the medial premotor areas not only showed a motor response component, but they also processed the visual and auditory information used as a metronome in a rhythmic tapping task. Note, however, that the classification was performed using only the inter-trial cell response consistency to the stimuli or tap events. We did not identify the visual or auditory receptive fields of cells, nor the cells' responses induced by joint manipulation, muscle tapping, or cutaneous stimulation.

TABLE 1. Number (and percentage) of cells that were classified as motor, sensory, complex and undetermined based on their γ values

Cell type	Visual	Auditory
Sensory	185 (30.5)	137 (25.4)
Complex	9 (1.5)	19 (3.5)
Motor	309 (50.9)	259 (48)
Undetermined	104 (17.1)	125 (23.1)
Total	607 (100)	540 (100)

We determined the position of the recording sites along the medial premotor areas relative to the brain sulci, using structural MRI (see Materials and methods). This analysis was carried out in order to test whether the cells classified as sensory in the present study showed a bias towards the pre-SMA, whereas motor cells showed a bias towards the SMA proper, as classical neurophysiological studies have previously demonstrated (Matsuzaka *et al.*, 1992). The results are shown in Fig. 3, where it is evident that cells classified as sensory in the visual and auditory conditions were mainly located in the pre-SMA, with a significant difference in their spatial distribution between the SMA proper and pre-SMA [visual: χ^2 test (1) = 6.4, $P = 0.011$; auditory: χ^2 test (1) = 7.3, $P = 0.007$]. Nevertheless, the cells classified as motor also showed a slight location bias towards the pre-SMA, with marginal differences between the two medial premotor areas [visual: χ^2 test (2.8) = 2.9, $P = 0.09$; auditory: χ^2 test (1) = 2.99, $P = 0.084$]. It is important to emphasise that the recording locations shown in Fig. 3 are approximated maps with a coarse spatial resolution (see Materials and methods). The proper spatial reconstruction of microelectrode trajectories requires the use of electrolytic lesions or coating the electrodes with a fluorescent dye, followed by the use of anatomical techniques in the postmortem tissue that allow the localisation of the lesions or fluorescent tracks (Matsuzaka *et al.*, 1992; Merchant *et al.*, 1997; Naselaris *et al.*, 2005). Unfortunately, we were not able to perform either of these methods in the present study.

Poisson-train analysis – finding the response profile of each cell

The response profile of each cell with respect to the stimuli or tapping movements was determined using the Poisson-train analysis, on the cells classified as sensory or motor in the previous time-warping section. This analysis determines how improbable it is that the number of action potentials within a specific time interval is a chance occurrence. For this purpose, the actual number of spikes within a time interval was compared with the number of spikes predicted by the Poisson distribution derived from the mean discharge rate across all conditions (see Materials and methods). Thus, the Poisson-train analysis essentially finds the response-onset latency and the extent of the periods of activation within each interval defined by two subsequent stimuli (sensory cells) (see Fig. 4) or two subsequent taps (motor cells) during the synchronisation phase of the SCT. In order to determine activation periods before and after each event, the Poisson-train analysis was carried out at 100 ms before the first event (stimulus or tap) and at 100 ms after the second event. Figure 5A shows the activation profiles of all sensory cells in the visual condition, where each row is associated with one neuron and the onset and extent of each activation period are illustrated as a horizontal line for the second serial-order element of the synchronisation phase and the 850 ms target interval. The cells were ordered according to their mean response-onset latency to the previous stimulus across all target intervals and serial-order elements. The Poisson-train analysis is quite stringent and only cells with consistent responses show significant activation periods. Consequently, the number of sensory and motor cells with significant activation periods is smaller than the original cells from the time-warping analysis, as shown in Table 2. It is crucial to emphasise that some cells, particularly in the sensory population, showed significant activation periods during both the visual and auditory conditions (audio-visual cells in Table 2). This result suggests that there was a small partial overlap in the sensory cell population processing the two modalities.

Visual and auditory responses – sensory-driven and stimulus-predicting activity

It is evident that the group of cells at the top of Fig. 5A showed shorter onset latencies than the cell group at the bottom. We used a hierarchical clustering analysis on the response-onset latencies of all of the cells, using the data for the second serial-order element of the synchronisation phase of the target interval of 850 ms (see Merchant *et al.*, 2003; Merchant & Georgopoulos, 2006). The results, shown in the dendrogram of Fig. 5B, indicate the existence of two large cell clusters (similar clustering was obtained using the other target intervals and serial-order elements). However, the hierarchical clustering is a descriptive method and therefore we used an algorithm using the expectation-maximisation clustering method on the mean response-onset and response-offset latencies across conditions. The expectation-maximisation was performed iteratively to obtain the

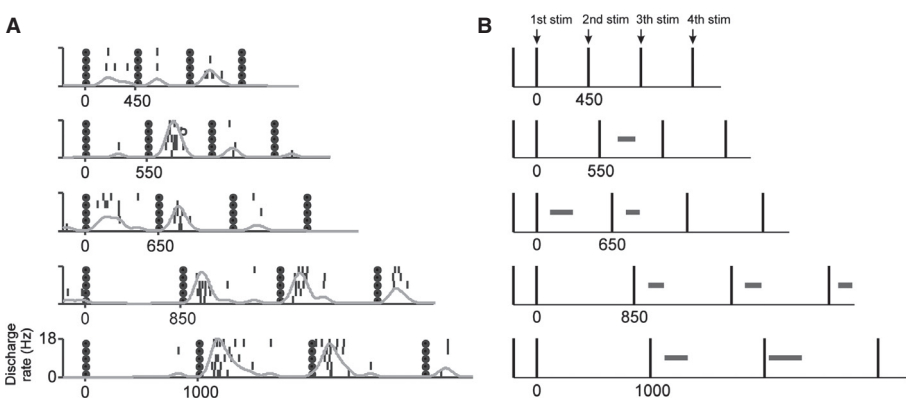

FIG. 4. Poisson-train analysis. (A) Raster plot of the activity of the cell shown in Fig. 2 and classified as sensory in the visual condition. Conventions as in Fig. 2. (B) Activation periods from the cell responses showed in A computed with the Poisson-train analysis.

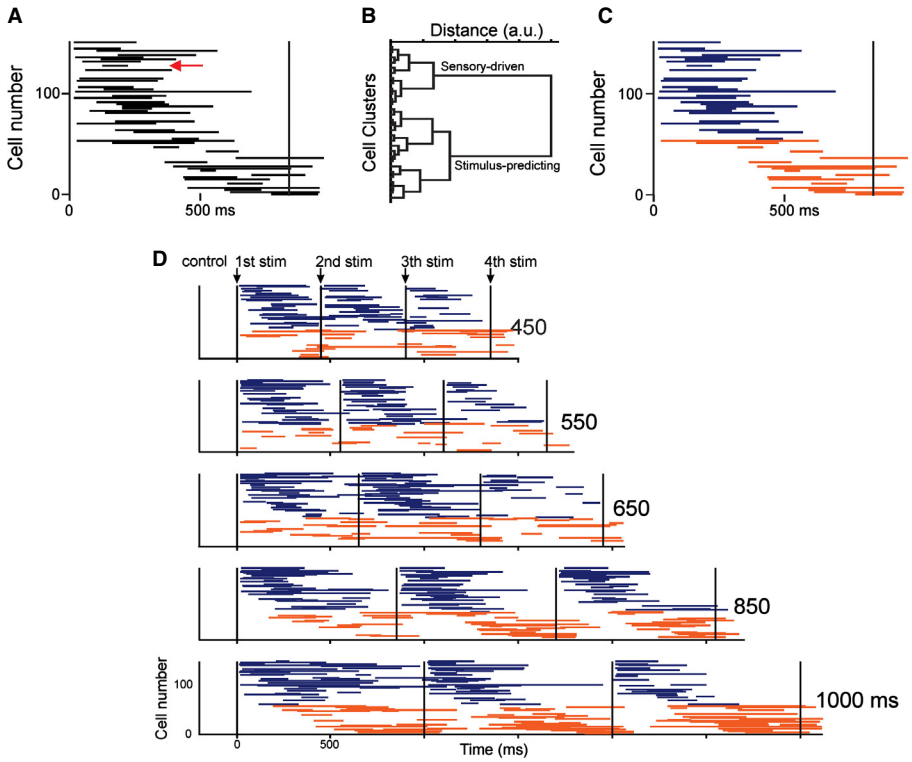

FIG. 5. Response profiles of sensory cells. (A) Response profiles for the cells with significant activation effects in the Poisson-train analysis. Each row is associated with one neuron and the onset and extent of each activation period are illustrated as a horizontal black line for the second serial-order element of the synchronisation phase and the 850 ms target interval. The red arrow is pointing at the visual sensory cell shown in the raster of Fig. 2. The black vertical lines correspond to the stimulus presentation. (B) Dendrogram of the hierarchical clustering using the response-onset latencies in A. The sensory-driven and stimulus-predicting large branches are specified. (C) The same activation profiles as in A are divided by the expectation-maximisation clustering results (see text for details). The blue color is for the sensory-driven cells and the orange for the stimulus-predicting cells. (D) Activation profiles of all of the sensory neurons across target intervals and serial-order elements of the synchronisation phase of the SCT in the visual condition. Again, the blue color is for the sensory-driven cells and the orange for the stimulus-predicting cells. a.u., arbitrary unit.

TABLE 2. Number of sensory and motor cells with consistent activation periods in the Poisson-train analysis

Cell type	Visual	Auditory	Audiovisual
Sensory	154	111	27
Motor	224	204	82

best clustering model using the Bayesian information criterion, testing different numbers of clusters and initial centroid and variance values. The best results were obtained with two clusters and the outcome is shown in Fig. 5C. One population of cells showed short response-onset latencies to the first stimulus (similar to the response to stimuli in sensory areas) and were therefore called sensory-driven neurons (Fig. 5C, blue). The other cell cluster was integrated by cells with long response onsets and with activity profiles that were probably predicting the occurrence of the next stimuli, instead of responding to the previous stimulus. This last group of cells was called stimulus-predicting neurons (Fig. 5C, orange).

We subsequently used the clustering outcome of Fig. 5C to identify the population response profile across all target intervals and serial-order elements. The results of this analysis are shown in Fig. 5D, where it is evident that the sensory-driven neurons showed similar activation profiles across target intervals and serial-order elements, whereas the stimulus-predicting neurons showed clear changes across target intervals. Interestingly, the sensory-driven neurons showed a significant decrease in the number of active cells as a function of the serial-order element [χ^2 test (2) = 12.1, $P = 0.002$], and a larger number of active cells in the visual than the auditory conditions [χ^2 test (1) = 9.9, $P = 0.002$] (see Fig. 6). In contrast, the number of active sensory-driven cells did not change as a function of target duration [χ^2 test (4) = 1.2, $P = 0.88$]. However, stimulus-predicting neurons did not show significant changes in the number of active cells as a function of the serial-order element [χ^2 test (2) = 0.7, $P = 0.7$], or between modalities [χ^2 test (1) = 0.99, $P = 0.32$], but showed a significant increase as a function of target duration [χ^2 test (4) = 23.1, $P < 0.0001$] (Fig. 6). These results suggest, first, that the sensory-driven neurons were more responsive to the first stimulus, and as the synchronisation phase was progressing to enter the internally-driven continuation phase, the cells were less engaged in responding to the incoming stimuli. On the contrary, the stimulus-predicting neurons were similarly engaged across serial-order elements. Second, sensory-driven neurons showed a clear bias toward the visual modality, in accordance with previous findings showing the bias of monkeys to process visual stimuli to guide their motor behavior (Zarco *et al.*, 2009; Nagasaka *et al.*, 2013; Honing & Merchant, 2014), whereas the number of activated stimulus-predicting neurons did not change across modalities. Finally, the target duration did not affect the number of active sensory-driven cells, but induced an increase in responding stimulus-predicting neurons, supporting the predictive nature of the latter group of cells, as there is an increase in expectation as time passes (Janssen & Shadlen, 2005).

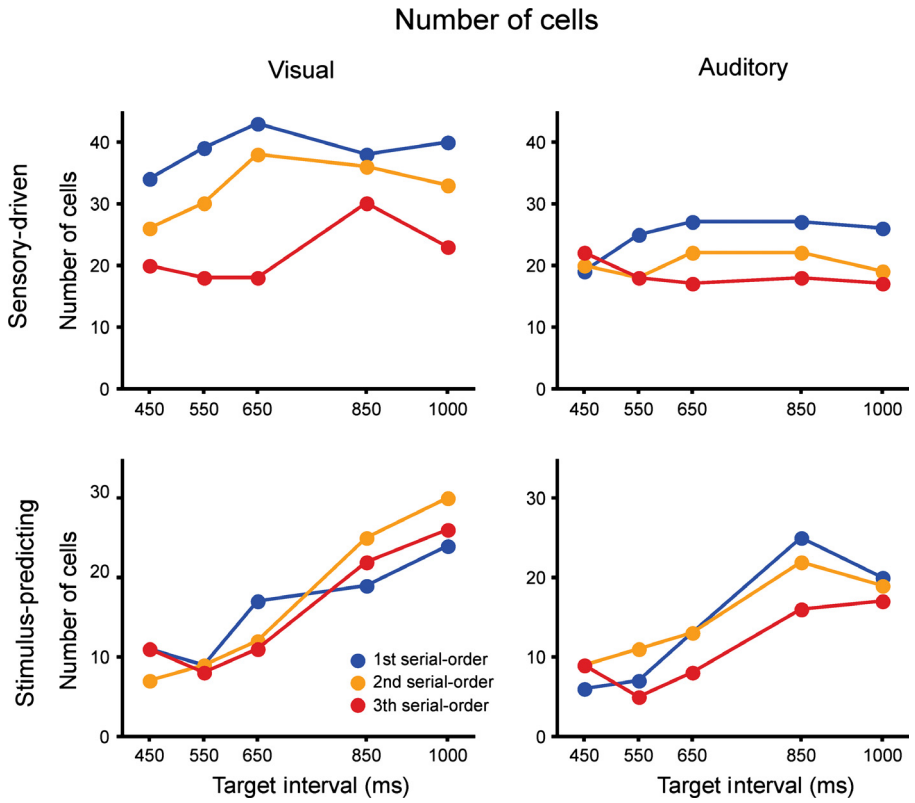

FIG. 6. Plots of the number of cells with significant effects in the Poisson-train analysis as a function of the target interval, and the serial-order element (color code in the inset), for the sensory-driven and stimulus-predicting cells, and for the visual and auditory conditions.

In addition, we performed an ANOVA where the target interval, serial order, and modality were the factors, and the dependent variable was the response-onset latencies with respect to the previous stimulus (Fig. 7). For the sensory-driven neurons, the ANOVA only showed a significant main effect for serial order ($F_{2,787} = 12.4$, $P < 0.0001$), with shorter latencies for the second and third elements of the serial order. It is notable that no differences were found in the response-onset latencies between modalities, indicating that the MPC has access to visual and auditory information at similar times from the presentation of a stimulus. The ANOVA for stimulus-predicting neurons showed significant main effects for serial order ($F_{2,398} = 4.63$, $P = 0.01$) (with shorter latencies for the second and third elements of serial order) and target interval ($F_{4,398} = 23.4.2$, $P < 0.0001$) (with a monotonic increment in onset latencies as a function of interval), but not modality ($F_{1,398} = 1.8$, $P = 0.18$). Finally, an additional ANOVA showed significant differences in response-onset latencies between sensory-driven and stimulus-predicting cells ($F_{1,1220} = 440$, $P < 0.0001$), where the former showed shorter response onsets.

We also analysed the response-onset latencies with respect to the next stimulus (Fig. 8). The results showed a significant strong linear increase in response latencies as a function of target interval for the sensory-driven cells ($F_{4,804} = 295.1$, $P < 0.0001$). This finding corroborates the idea that sensory-driven cells were tied to the previous stimulus with constant response-onset latencies to the previous stimulus and linearly varying latencies to the next stimulus as a function of target interval. In contrast, the response-onset latencies to the next stimulus showed a smaller increment as a function of target interval in stimulus-predicting cells. Although in this case the ANOVA also showed a significant main effect for target interval ($F_{4,415} = 30.7$, $P < 0.0001$), the slope of the linear regression between the response latencies to the next stimulus and the target interval was significantly larger in sensory-driven (mean slope 0.98, $R^2 = 0.61$) than in stimulus-predicting (mean slope 0.48, $R^2 = 0.2$) cells (Fig. 8) in an ANOVA analysis (see Zar, 1999) ($F_{1,702} = 17.5$, $P < 0.0001$). Therefore, the response onset of stimulus-predicting cells was probably dictated by an interaction between the duration of the activation profile associated with the increase in expectation as time passes, and the onset of the prediction process linked to the next stimulus presentation.

Overall, these analyses support the notion of two populations of sensory cells, one responding to the incoming sensory information when it is used to drive the periodic tapping of the monkeys, and another that predicts the appearance of the next stimulus in a rhythmic sequence of sensorimotor events.

Motor responses – a coordinated gradient of activation profiles

There was a gradual and dynamic profile in the onset–offset of the activation patterns of motor cells. Figure 9A shows the activation profiles with respect to movement taps for all motor cells in the visual condition for the second serial-order element and the 850 ms target duration. The response profiles were ordered according to their mean response-onset latencies from the previous tap times across all target intervals and serial-order elements. Thus, the cells in blue were active just before the first tap in that serial-order element and it seems that they pass the information to the cells in green, so that there is a gradient of cell activation throughout the interval, with the red cells being activated before and after the second tap. The activation gradients of motor cells are quite different from the two-cluster behavior of sensory cells. In fact, the best results of the expectation-maximisation clustering using the

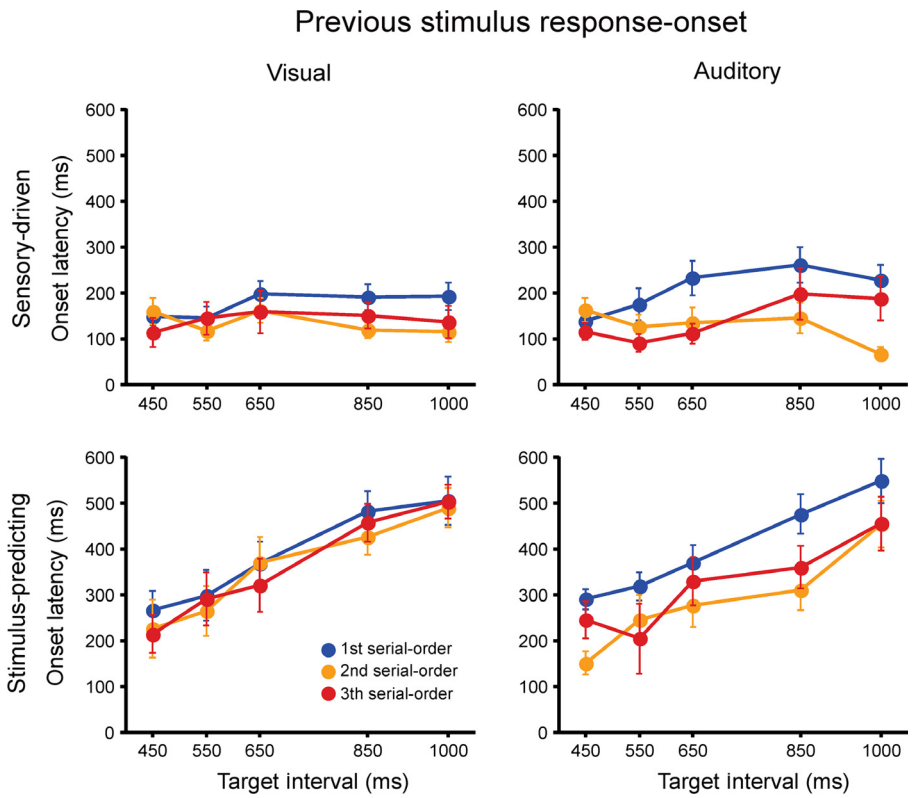

FIG. 7. Plots of the response-onset latency to the previous stimulus in cells with significant effects in the Poisson-train analysis as a function of the target interval, and the serial-order element (color code in the inset), for the sensory-driven and stimulus-predicting cells, and for the visual and auditory conditions.

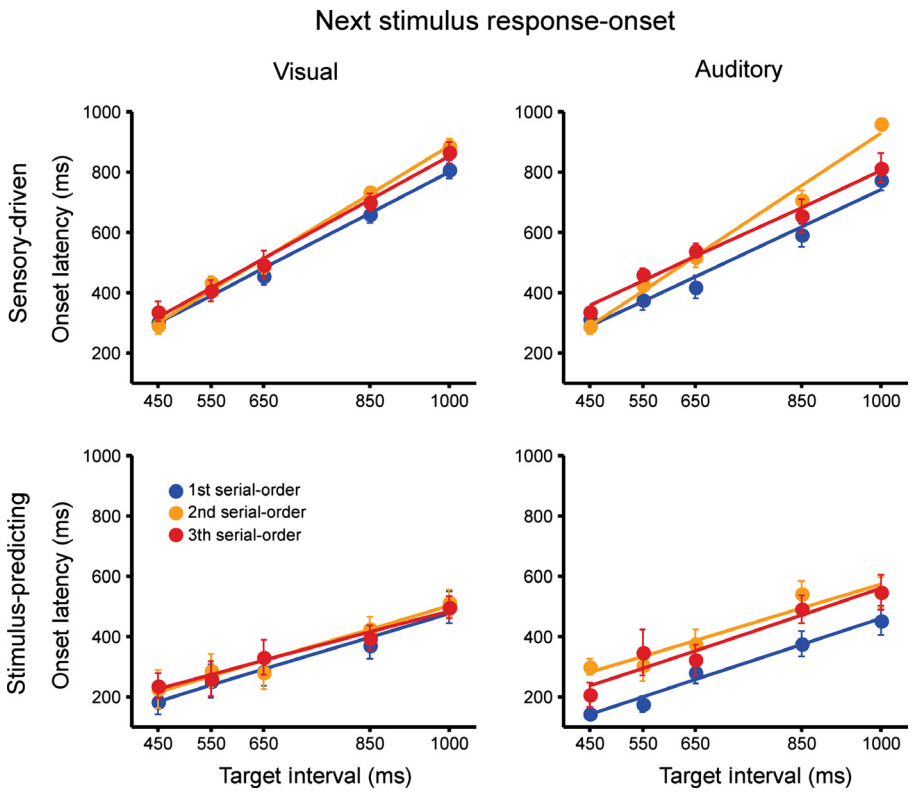

FIG. 8. Plots of the response-onset latency to the next stimulus in cells with significant effects in the Poisson-train analysis as a function of the target interval, and the serial-order element (color code in the inset), for the sensory-driven and stimulus-predicting cells, and for the visual and auditory conditions. Continuous colored lines correspond to the best linear regression model for the data of each serial-order element.

Bayesian information criterion were obtained with four clusters, suggesting the existence of a continuous pattern of activation profiles rather than two clusters as in the case of sensory cells. Hence, we used a two-dimensional normal distribution in order to characterise the cell activation gradients across all combinations of target intervals and the serial-order elements. From the normal distribution that has an elliptical shape (Fig. 9A), we can extract the important parameters associated with the larger ellipse diameter (called the normal distribution vector). These parameters are: δ, which is the vector length, θ, which is the vector angle, and τ, which is the latency to the vector's superior-left peak (Fig. 9B). These parameters define the dynamic pattern of activation profiles among conditions. Figure 9C shows the activation profiles of all of the motor neurons across target intervals and serial-order elements of the synchronisation phase of the SCT in the visual condition. This figure shows that the cells in blue were active just before the first tap of the corresponding serial-order element. The blue cells seem to pass the information to the green/yellow cells, forming a gradient of cell activation throughout the interval that ends with the red cells that were activated before and after the second tap of the corresponding serial-order element. These gradients are particularly evident for longer durations and the second and third serial-order elements of the SCT sequence. In addition, Fig. 9C shows that the two-dimensional normal distribution characterises properly the dynamic profile of activation of the motor cells across all of the target interval/serial-order element combinations. It also shows that the elliptical shape of these distributions changed with the experimental conditions. Indeed, the response-onset latencies of motor cells showed significant changes as a function of target interval ($F_{4,2782}$ = 35.5, P < 0.0001) and serial order ($F_{2,2782}$ = 6.6, P = 0.001), but were similar between modalities ($F_{1,2782}$ = 3.2, P = 0.074). In addition, motor cells showed significant main effects in their response duration for serial order ($F_{2,2782}$ = 34.1, P < 0.0001) and target interval ($F_{4,2156}$ = 13.3, P < 0.0001), and again were similar between modalities ($F_{1,2782}$ = 1.89, P = 6.66) (Fig. 11A). Finally, Fig. 9C depicts a cyclical configuration of these activation patterns, so that once a serial-order element is finished, a similar activation gradient starts again in the next element.

The cyclical configuration of the population activation patterns is more evident in Fig. 10A and B, where the normal distribution vectors were plotted as a function of target interval and serial-order element. Furthermore, the dotted lines in Fig. 10A and B exemplify a hypothetical connection between the last group of cells activated at the end of one serial-order element, and the first group of cells activated at the beginning of the next element. These hypothetical connections would be highly coordinated for target intervals above 550 ms, as the beginning and end of the normal distribution vectors overlapped with their corresponding initial and following taps. Conversely, the beginning of the normal distribution vectors for shorter durations start almost in the middle of each interval, reflecting a strong bias in the pattern of activation for the next tap (i.e. tap prediction). Accordingly, the length of the normal distribution vectors δ increased (Fig. 11B) and the peak latency τ decreased (Fig. 11C) as a function of the target duration and the serial order. It is of importance that the cyclical configuration of activation patterns showed a progressive and significant increase in the number of responding cells as the serial-order elements evolved [χ^2 test (2) = 6.2, P = 0.046] (Fig. 10C and D). In addition, there was a significant increase in the number of active motor cells as a function

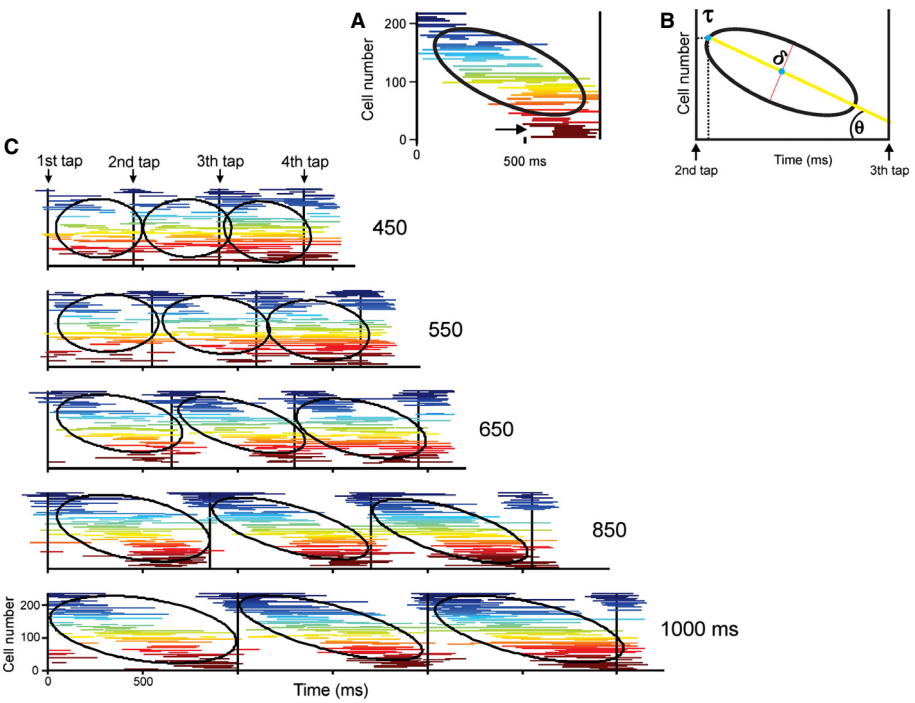

FIG. 9. Response profiles of motor cells. (A) Response profiles for the cells with significant activation effects in the Poisson-train analysis during the second serial-order element of the synchronisation phase and the 850 ms target interval. The black vertical lines correspond to the time of the taps. The black arrow points to the response-onset latency and the extent of the periods of activation for the visual motor cell shown in Fig. 2. The black ellipse is the normal distribution for the activity profiles of all cells. (B) Normal distribution parameters from the vector (normal distribution vector) associated with the larger ellipse diameter. δ, vector length; θ, vector angle; τ, latency to the vector's superior-left peak. (C) Activation profiles of all of the motor neurons across target intervals and serial-order elements of the synchronisation phase of the SCT in the visual condition. The color code used in the activation profiles of cells is to highlight the continuum in the response-onset latencies of motor cells.

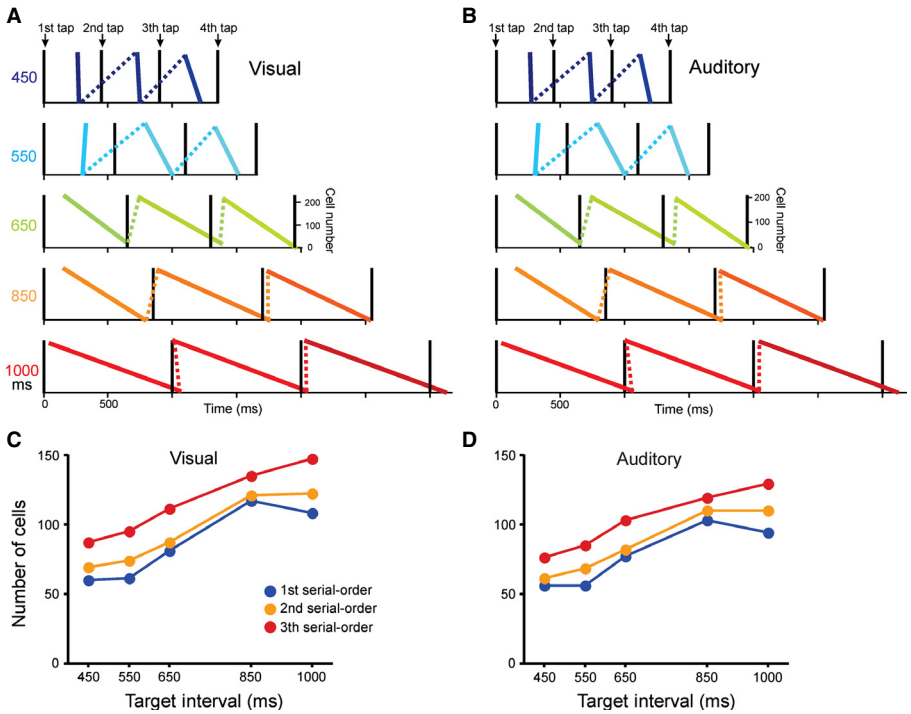

FIG. 10. Normal distribution vectors of motor cells across target intervals and serial-order elements for the visual (A) and auditory (B) conditions. Plots of the number of motor cells with significant effects in the Poisson-train analysis as a function of the target interval, and the serial-order element (color code in the inset) for the visual (C) and auditory (D) conditions.

of target interval [χ^2 test (4) = 21, $P < 0.0001$], and the number of active motor cells was similar between the visual and auditory conditions [χ^2 test (1) = 1.1, $P = 0.28$] (Fig. 10C and D). In sum, these findings support the idea that the cyclical configuration of the activation dynamics recruited more motor cells as the serial-order elements progressed across the synchronisation phase of the SCT.

The rate at which the cells were recruited over time is captured by the angle θ of the normal distribution vector (Fig. 9B), which makes this parameter a fundamental variable to study cell ensemble dynamics. The angle θ (Fig. 11D) showed a significant increase as a function of target interval (ANOVA on regression slopes, see Zar, 1999) for the visual ($F_{3,65026} = 58.3$, $P < 0.0001$) and auditory ($F_{3,59826} = 150.6$, $P < 0.0001$) conditions, and also as a function of serial order (visual: $F_{1,149226} = 410.1$, $P < 0.0001$; auditory: $F_{1,131635} = 173.2$, $P < 0.0001$), but was similar between modalities [t-test(575516) = 0.22, $P = 0.54$].

In conclusion, the cells classified as motor in the time-warping analysis show a cyclical configuration of activation gradients, where the number of recruited cells in these gradients increases as a function of the serial-order elements and the rate of cell engagement over time in the population dynamics decreases as a function of the target interval. The coordinated activation profiles of cell populations were similar between the modalities tested.

Sensory and motor cells encode temporal and sequential information

We performed a two-way ANOVA, where the target interval and the serial-order element of the SCT during the synchronisation phase were the factors and where the discharge rate of the sensory or motor cells was the dependent variable. Table 3 shows the number of cells with significant main effect or the interaction for target interval × serial order for all of the cell types studied in the present study. It is clear that sensory-driven, stimulus-predicting, and motor cells encoded the temporal and sequential information, as previously reported for cells multiplexing these parameters in their tuning functions (Merchant *et al.*, 2013b).

Discussion

We determined the response properties of MPC cells that were classified as sensory or motor during a task that involved isochronous tapping to a sensory metronome. The classification was based on a warping transformation (Perez *et al.*, 2013) that allowed us to statistically determine whether the activity of a cell was better aligned to sensory or motor events during the synchronisation phase of the SCT. We found that a large proportion of cells were categorised as either sensory or motor, suggesting that the medial premotor areas not only show a motor response component, but also process brief visual or auditory stimuli used as a metronome in a rhythmic tapping task. The recording location of both cell types was biased towards the pre-SMA, particularly for sensory cells. We then characterised the response-onset latency and the extent of the activation periods within each interval defined by two subsequent stimuli (sensory cells) or two subsequent taps (motor cells). Two distinctive clusters of sensory cells were observed, i.e. one cell population with short response-onset latencies to the previous stimulus (called sensory-driven neurons), and another that included cells with long response-onsets and with activity profiles that were probably predicting the occurrence of the next stimuli, instead of responding to the previous stimulus (called stimulus-predicting neurons). Sensory-driven neurons showed a clear bias towards the visual modality and were more responsive to the first stimulus, so that as the synchronisation phase progressed, the cells were less engaged in responding to the incoming stimuli. In contrast,

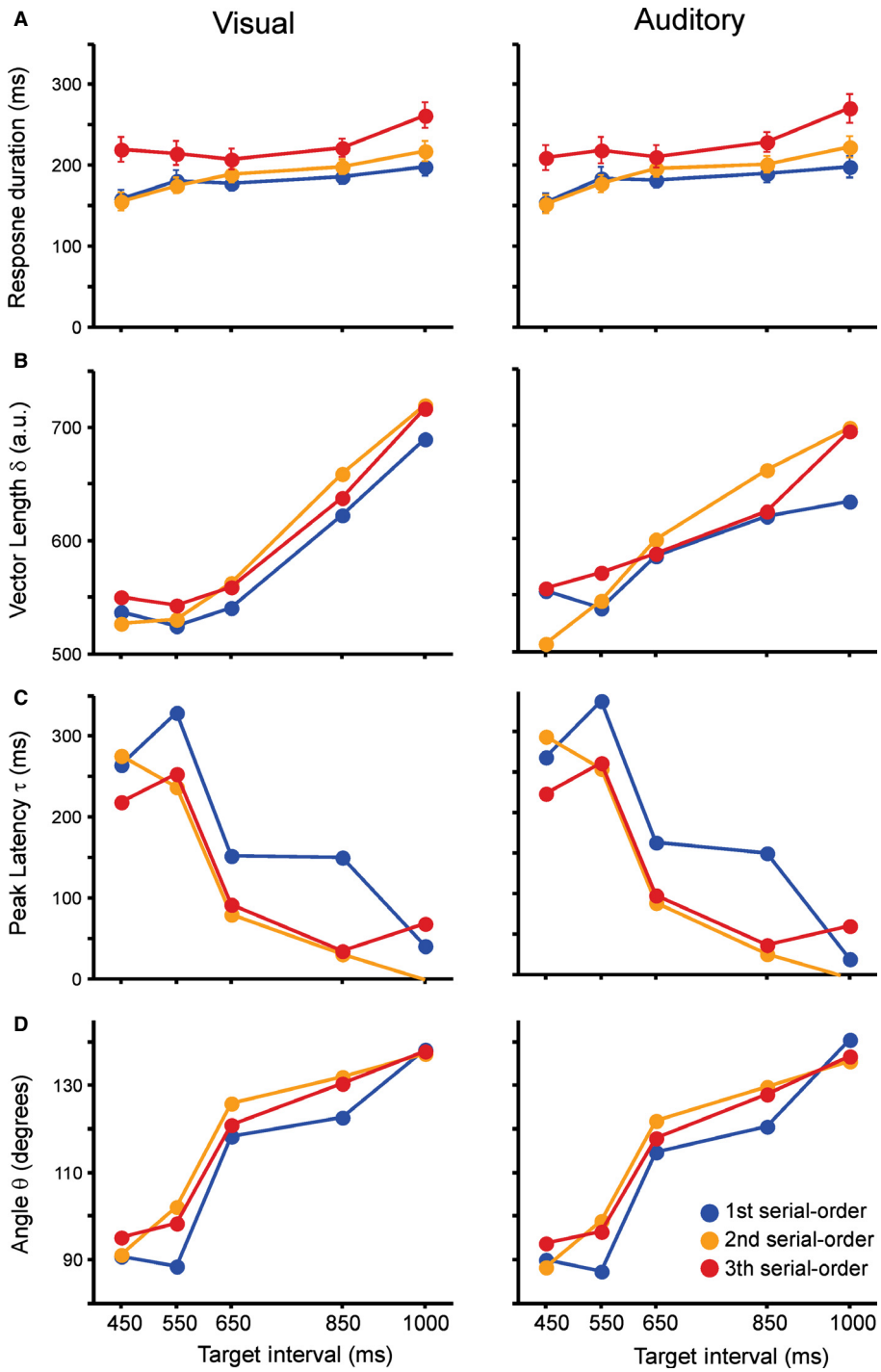

FIG. 11. (A) Plots of the response duration of the motor cells with significant effects in the Poisson-train analysis as a function of the target interval, and the serial-order element (color code in the inset). (B) Length δ of the normal distribution vectors of motor cells as a function of the target interval, and the serial-order element. (C) Peak latency τ of the normal distribution vectors of motor cells as a function of the target interval, and the serial-order element. (D) Angle θ of the normal distribution vectors of motor cells as a function of the target interval, and the serial-order element. Visual condition on the left, auditory condition on the right. a.u., arbitrary unit.

stimulus-predicting neurons were bimodal and showed similar response profiles across serial-order elements. However, the motor cells showed a consecutive onset in the activity of discrete neural ensembles, generating a rapid succession of neural events between the two taps defining a produced interval. This dynamic chain of neural events occurred for each element of the task synchronisation phase, resulting in a cyclical recruitment of similar activation profiles across the sequential structure of the isochronous tapping. However, the rate of cell recruitment over time in the population dynamics decreased and was more coordinated as a function of the target interval. In addition, the cyclical configuration in activation profiles engaged more motor cells as the serial-order elements progressed across the synchronisation phase of the SCT. These findings support the notion that motor cells are responsible for the rhythmic progression of movements

TABLE 3. Number of sensory and motor cells with responses that showed significant effects for target interval or serial order in a two-way ANOVA

Cell type	Interval	Serial order
Sensory-driven A	40	45
Sensory-driven V	64	74
Stimulus-predicting A	26	27
Stimulus-predicting V	35	44
Motor V	152	191
Motor A	127	148

A, auditory; V, visual condition.

in the task, gaining more importance as the trial evolves, whereas, simultaneously, the sensory-driven cells lose their functional influence.

The recording locations of both sensory and motor cells in the present study, according to our structural MRI reconstructions, were biased towards the pre-SMA particularly for the first type of cells. In contrast, Matsuzaka *et al.* (1992) demonstrated that the SMA proper is mainly responsible for: (i) evoked movements by intracortical microstimulation, (ii) passive somatosensory responses, and (iii) phasic premovement activity during a motor task, whereas the pre-SMA shows a strong a bias towards task-induced visual responses. Subsequent anatomical and neurophysiological studies have supported the existence of the two distinct medial premotor areas (i.e. Alexander & Crutcher, 1990; Luppino *et al.*, 1993). Although some of the cell responses described in the present study could be classified in terms of classic sensory or motor responses, many lines of evidence suggest that these cells are engaged in cognitive rather than traditional sensorimotor functions. First, a large proportion of our motor cells were recorded in the pre-SMA, suggesting that some of them may not show the motor properties described in previous articles (Matsuzaka *et al.*, 1992). Second, most of the sensory and motor cells encoded the duration and serial order of the intervals produced in the SCT (Table 3), suggesting their role in encoding cognitive parameters of the task. Third, there was a decrease in the number of engaged sensory-driven neurons as the serial-order elements progressed in the SCT, accompanied by a decrease in their response-onset latencies to the previous stimulus event. Hence, these were not classical sensory cells, and probably their sensory input arose from the posterior parietal cortex, which in turn could have been modulated centrally to prepare the circuit for the upcoming internally driven continuation phase of the task, as shown previously in other paradigms (Merchant *et al.*, 2011a; Crowe *et al.*, 2013). Finally, the responses of motor cells that were activated after the taps also showed a strong serial-order effect, where the number of active cells was larger for the second and third elements of the SCT sequence, which is not the behavior of cells with passive somatosensory responses (Romo *et al.*, 1997). We discuss these issues in the following paragraphs.

Rhythmic entrainment refers to the ability to align motor actions with an auditory beat, where a beat corresponds to the perceived pulse that marks equally spaced points in music or a sequence of auditory stimuli (Large & Palmer, 2002; Honing, 2012; Merchant & Honing, 2014). In humans, rhythmic entrainment is a common and widespread behavior that involves timed movements of different body parts (such as finger or foot taps, or body sway). Indeed, the majority of human listeners can easily synchronise (with no training) at rates that are integer multiples or fractions of the basic beat (Large & Jones, 1999). Thus, rhythmic entrainment is a fundamental element of music behavior and has a clear bias towards the auditory modality (Grondin *et al.*, 1996; Merchant *et al.*, 2008a; Grahn, 2012; Hove *et al.*, 2013a; Honing & Merchant, 2014); for a long time this was thought to be an exclusive trait of humans beings (Patel, 2014). The synchronisation phase of the SCT is the simplest case of rhythmic entrainment, as the beat is isochronous, and has been extensively used to study the neural underpinnings of rhythmic behavior. Humans differ substantially in their entrainment abilities from other primates (Merchant & Honing, 2014). Monkeys, for example, do not appear to spontaneously move to the beat of a musical rhythm. Nevertheless, monkeys are able to produce rhythmic movements with proper tempo matching during the SCT (which constitutes a simple isochronous challenge for humans). Indeed, monkeys produced isochronous rhythmic movements by temporalising the pause between movements and not the duration of their movement (Donnet *et al.*, 2014). These results indicate that monkeys use an explicit timing strategy to perform the SCT, where the timing mechanism controlled the duration of the movement pauses, which also triggered the execution of stereotyped pushing movements across each produced interval in the rhythmic sequence. However, macaques do not seem to have the refined prediction abilities of humans during rhythmic entrainment and show better performance in the SCT using visual rather than auditory cues, contrary to the auditory bias in humans (Honing & Merchant, 2014). The present results indicate a larger number of sensory-driven neurons responding to visual rather than auditory metronomes. Hence, the large visual input from the posterior parietal areas (particularly area PFG) to the MPC (Luppino *et al.*, 1993) can be used to generate an initial sensory signal in the motor system to generate subsequent predictive sensory signals. In contrast, the auditory information also coming from the posterior parietal areas seems to drive the activity of a smaller MPC cell network (Uhrig *et al.*, 2014), even if the response-onset latencies of sensory-driven neurons to stimuli of both modalities were similar. Consequently, this discrepancy could explain the monkeys' bias towards visual stimuli when driving their rhythmic behavior. In turn, we can speculate that the strong auditory input to the premotor system in humans (Hove *et al.*, 2013b), coming through a larger arcuate and superior longitudinal fasciculus than in monkeys (Rilling *et al.*, 2008), is a key element for the auditory bias in music behavior in *Homo sapiens* (Mendoza & Merchant, 2014). It is important to emphasise that neural responses in the MPC, similar to the reported sensory-driven neurons, have been recorded using visual, tactile, and auditory stimuli in tasks where a single stimulus cued a monkey motor response using a particular rule (Kurata & Tanji, 1985; Tanji & Kurata, 1985; Romo & Schultz, 1987; Romo *et al.*, 1993, 1997; Merchant *et al.*, 2001, 2004a). In contrast, when the same stimulus is presented in a passive context, the associated sensory responses are not observed (Tanji & Kurata, 1982; Kurata & Tanji, 1985). These findings suggest that the monkeys need to be focused on a task using the stimulus to drive their behavior in order to observe the sensory driven activity in the MPC. A note of precaution is in order here. Our time-warping method gives a statistical measure of the response alignment to sensory or motor events during a sensorimotor sequential task. Nevertheless, additional neurophysiological procedures are needed to define whether a cell classified as sensory with the warping method indeed has a sensory receptive field and encodes the physical properties of the incoming stimulus (Romo *et al.*, 1996; de Lafuente & Romo, 2006).

We can also speculate that, through the intensive training in the SCT (Zarco *et al.*, 2009), the initial sensory-driven responses of the MPC in the monkey may have been linked to neurons triggering the tapping behavior. This initial sensorimotor association started by sending a motor command in order to react to each stimulus, and

was then probably transformed to generate a predictive sensory signal in order to produce tapping responses closer to the stimulus onset. In fact, the time between the stimuli and the taps of trained monkeys in the SCT are shorter than their reaction times in a control task with random inter-stimulus intervals, suggesting that monkeys do have temporal prediction capabilities during the SCT (Zarco *et al.*, 2009). We suggest that the monkey prediction abilities in the SCT depend on the stimulus-predicting neurons found in the present study, which were bimodal and showed similar response profiles across serial-order elements. In previous studies we found that the motor system processes visual information of a moving target in a predictive fashion in order to trigger a single interception movement (Merchant *et al.*, 2004a,b; Merchant & Georgopoulos, 2006). Hence, the learning process of behaviors that need temporal prediction, such as target interception, collision avoidance, and rhythmic entrainment, probably generates sensory prediction signals in the motor cortical system (Merchant *et al.*, 2009, 2011a). It has been reported that human beta oscillations are crucial for predictive timing in auditory beat processing, and that beta oscillations involve top-down interactions between motor and auditory regions (Fujioka *et al.*, 2009, 2012). The beta signals tracked the tempo of the stimulus beat and predicted the onset of the following beat (Fujioka *et al.*, 2012). Furthermore, beta oscillations in the motor cortico-thalamic-basal ganglia circuit are involved in processing predictive temporal information during both the SCT (Bartolo *et al.*, 2014) and the presentation of auditory stimuli with complex metrics (Iversen *et al.*, 2009). Overall, these observations support the idea that the sensory prediction signals may not only interact with the neural apparatus present in the motor cortical system for the activation of predictive motor commands, but also generate top-down signals to sensory areas in order to efficiently process the incoming sensory information during rhythmic entrainment.

The cells classified as motor in the present study showed an organised and sequential onset in activity, so that the groups of active neurons changed dramatically within the two taps defining a produced interval. Hence, these neural responses are qualitatively different from the traditional movement preparation and execution signals in the motor and premotor areas of the cortex (Tanji & Evarts, 1976; Georgopoulos *et al.*, 1982, 2007; Tanji & Kurata, 1982; Wise, 1985; Naselaris *et al.*, 2006). Recently, we demonstrated that the MPC cells that encode the duration and the serial order in the SCT showed similar activation dynamics (Crowe *et al.*, 2014; Merchant *et al.*, 2015), suggesting that the motor cells of the present study constitute the main cell type reported in the previous article. In the present study, however, the dynamic chain of neural events occurred within each element of the task synchronisation phase, resulting in a cyclical recruitment of cell populations with similar activation profiles across the sequential structure of the task (Buonomano & Laje, 2010; Goel & Buonomano, 2014). This cyclical repetition of activation profiles within each produced interval can be the neural substrate for the rhythmic progression of movements during isochronous tapping to a sensory metronome. We suggest that the cyclical repetition of response profiles has an anatomofunctional substrate, where the neuronal ensembles are arranged in inter-connected modules, providing a strong synaptic drive to the next ensemble, and producing a recurring flow of information along a chain of neural ensembles (Gewaltig *et al.*, 2001). This hypothesis is supported by the recent observation that the magnitude of baseline activity correlations among cell pairs, which is an indirect measure of synaptic relations between the simultaneously recorded cells (de la Rocha *et al.*, 2007), shows a cyclical organisation along the elements of the SCT task sequence (Crowe *et al.*, 2014).

The rate of cell recruitment over time in the population dynamics decreased as a function of the target interval, again supporting the idea that the temporal structure of the SCT depends on these dynamic population code. Furthermore, we observed that the cyclical activation profiles engaged more motor cells as the serial-order elements progressed across the synchronisation phase of the SCT. This last finding corroborates the notion that the cells classified as motor in the present article could define the rhythmic evolution of movements in the task, gaining more importance as the trial progressed, whereas the sensory metronome was less important and the corresponding input from sensory-driven cells became less preponderant.

To finish, we also found that sensory-driven, stimulus-predicting, and motor cells encoded the temporal and sequential information, as previously reported for MPC cells multiplexing these parameters in their tuning functions (Merchant *et al.*, 2013b). Therefore, the dynamic response profiles of cells associated with the sensory, sensorimotor, and motor aspects of the synchronisation phase of the SCT include another dimension of neural processing, i.e. the duration and the element in the sequence that is being performed. We can infer that an intricate set of dynamic interactions between these cell types is needed in order to perform the isochronous tapping to a sensory metronome. The nature of these interactions, however, is out of the reach of the present article, as a large amount of simultaneously recorded cells is required to determine synaptic interactions and the dynamic transfer of information within and between neural circuits (Fujisawa *et al.*, 2008; Merchant *et al.*, 2011b, 2014; Berényi *et al.*, 2014). Thus, experiments using multiple chronic microelectrodes in animals performing the SCT are in progress.

Acknowledgements

This research was supported by CONACYT (151223) and PAPIIT (IN201214-25). We thank Victor de Lafuente for his fruitful comments on the manuscript. We also thank Raúl Paulín and Juan José Ortiz for their technical assistance. The authors declare no conflict of interest.

Abbreviations

MPC, medial premotor cortex; MRI, magnetic resonance imaging; preSMA, pre-supplementary motor area; SCT, synchronisation-continuation task; *SI*, surprise index; SMA, supplementary motor area proper.

References

Alexander, G.E. & Crutcher, M.D. (1990) Preparation for movement: neural representations of intended direction in three motor areas of the monkey. *J. Neurophysiol.*, **64**, 133–150.

Bartolo, R., Prado, L. & Merchant, H. (2014) Information processing in the primate basal ganglia during sensory guided and internally driven rhythmic tapping. *J. Neurosci.*, **34**, 3910–3923.

Bengtsson, S.L., Ehrsson, H.H., Forssberg, H. & Ullén, F. (2005) Effector-independent voluntary timing: behavioural and neuroimaging evidence. *Eur. J. Neurosci.*, **22**, 3255–3265.

Berényi, A., Somogyvári, Z., Nagy, A.J., Roux, L., Long, J.D., Fujisawa, S., Stark, E., Leonardo, A., Harris, T.D. & Buzsáki, G. (2014) Large-scale, high-density (up to 512 channels) recording of local circuits in behaving animals. *J. Neurophysiol.*, **111**, 1132–1149.

Buhusi, C.V. & Meck, W.H. (2005) What makes us tick? Functional and neural mechanisms of interval timing. *Nat. Rev. Neurosci.*, **6**, 755–765.

Buonomano, D.V. & Laje, R. (2010) Population clocks: motor timing with neural dynamics. *Trends Cogn. Sci.*, **14**, 520–527.

Coull, J.T., Cheng, R.K. & Meck, W.H. (2011) Neuroanatomical and neurochemical substrates of timing. *Neuropsychopharmacology*, **36**, 3–25.

Crowe, D.A., Goodwin, S.J., Blackman, R.K., Sakellaridi, S., Sponheim, S.R., MacDonald, A.W. III & Chafee, M.V. (2013) Prefrontal neurons transmit signals to parietal neurons that reflect executive control of cognition. *Nat. Neurosci.*, **16**, 1484–1491.

Crowe, D.A., Zarco, W., Bartolo, R. & Merchant, H. (2014) Dynamic representation of the temporal and sequential structure of rhythmic movements in the primate medial premotor cortex. *J. Neurosci.*, **34**, 12660–12671.
Dhamala, M., Pagnoni, G., Wiesenfeld, K., Zink, C.F., Martin, M. & Berns, G.S. (2003) Neural correlates of the complexity of rhythmic finger tapping. *NeuroImage*, **20**, 918–926.
Donnet, S., Bartolo, R., Fernandes, J.M., Cunha, J.P., Prado, L. & Merchant, H. (2014) Monkeys time their movement pauses and not their movement kinematics during a synchronization-continuation rhythmic task. *J. Neurophysiol.*, **111**, 2250–2257.
Fujioka, T., Trainor, L.J., Large, E.W. & Ross, B. (2009) Beta and gamma rhythms in human auditory cortex during musical beat processing. *Ann. NY Acad. Sci.*, **1169**, 89–92.
Fujioka, T., Trainor, L.J., Large, E.W. & Ross, B. (2012) Internalized timing of isochronous sounds is represented in neuromagnetic beta oscillations. *J. Neurosci.*, **32**, 1791–1802.
Fujisawa, S., Amarasingham, A., Harrison, M.T. & Buzsáki, G. (2008) Behavior-dependent short-term assembly dynamics in the medial prefrontal cortex. *Nat. Neurosci.*, **11**, 823–833.
Georgopoulos, A.P., Kalaska, J.F., Caminiti, R. & Massey, J.T. (1982) On the relations between the direction of two-dimensional arm movements and cell discharge in primate motor cortex. *J. Neurosci.*, **2**, 1527–1537.
Georgopoulos, A.P., Merchant, H., Naselaris, T. & Amirikian, B. (2007) Mapping of the preferred direction in the motor cortex. *Proc. Natl. Acad. Sci. USA*, **104**, 11068–11072.
Gewaltig, M.O., Diesmann, M. & Aertsen, A. (2001) Propagation of cortical synfire activity: survival probability in single trials and stability in the mean. *Neural Networks*, **14**, 657–673.
Goel, A. & Buonomano, D.V. (2014) Timing as an intrinsic property of neural networks: evidence from in vivo and in vitro experiments. *Philos. T. Roy. Soc. B.*, **369**, 20120460.
Grahn, J.A. (2012) See what I hear? Beat perception in auditory and visual rhythms. *Exp. Brain Res.*, **220**, 51–61.
Grondin, S. (2001) From physical time to the first and second moments of psychological time. *Psychol. Bull.*, **127**, 22–44.
Grondin, S., Ivry, R.B., Franz, E., Perreault, L. & Metthe, L. (1996) Markers' influence on the duration discrimination of intermodal intervals. *Percept. Psychophys.*, **58**, 424–433.
Hanes, D.P., Thompson, K.G. & Schall, J.D. (1995) Relationship of presaccadic activity in frontal eye field and supplementary eye field to saccade initiation in macaque: Poisson spike train analysis. *Exp. Brain Res.*, **103**, 85–96.
Honing, H. (2012) Without it no music: beat induction as a fundamental musical trait. *Ann. NY Acad. Sci.*, **1252**, 85–91.
Honing, H. & Merchant, H. (2014) Differences in auditory timing between human and non-human primates. *Behav. Brain Sci.* **37**.
Hove, M.J., Iversen, J.R., Zhang, A. & Repp, B.H. (2013a) Synchronization with competing visual and auditory rhythms: bouncing ball meets metronome. *Psychol. Res.*, **77**, 388–398.
Hove, M.J., Fairhurst, M.T., Kotz, S.A. & Keller, P.E. (2013b) Synchronizing with auditory and visual rhythms: an fMRI assessment of modality differences and modality appropriateness. *NeuroImage*, **67**, 313–321.
Iversen, J.R., Repp, B.H. & Patel, A.D. (2009) Top-down control of rhythm perception modulates early auditory responses. *Ann. NY Acad. Sci.*, **1169**, 58–73.
Ivry, R.B. & Hazeltine, R.E. (1995) Perception and production of temporal intervals across a range of durations: evidence of a common timing mechanism. *J. Exp. Psychol. Human.*, **21**, 3–18.
Janata, P. & Grafton, S.T. (2003) Swinging in the brain: shared neural substrates for behaviors related to sequencing and music. *Nat. Neurosci.*, **6**, 682–687.
Janssen, P. & Shadlen, M.N. (2005) A representation of the hazard rate of elapsed time in macaque area LIP. *Nat. Neurosci.*, **8**, 234–241.
Kass, R.E. & Raftery, A.E. (1995) Bayes factors. *J. Am. Stat. Assoc.*, **90**, 773–795.
Kurata, K. & Tanji, J. (1985) Contrasting neuronal activity in supplementary and precentral motor cortex of monkeys. II. Responses to movement triggering vs. nontriggering sensory signals. *J. Neurophysiol.*, **53**, 142–152.
de Lafuente, V. & Romo, R. (2006) Neural correlate of subjective sensory experience gradually builds up across cortical areas. *Proc. Natl. Acad. Sci. USA*, **103**, 14266–14271.
Large, E.W. & Jones, M.R. (1999) The dynamics of attending: how people track time-varying events. *Psychol. Rev.*, **106**, 119–159.
Large, E.W. & Palmer, C. (2002) Perceiving temporal regularity in music. *Cognitive Sci.*, **26**, 1–37.
Lewis, P.A., Wing, A.M., Pope, P.A., Praamstra, P. & Miall, R.C. (2004) Brain activity correlates differentially with increasing temporal complexity of rhythms during initialisation, synchronisation, and continuation phases of paced finger tapping. *Neuropsychologia*, **42**, 1301–1312.
Luppino, G., Matelli, M., Camarda, R. & Rizzolatti, G. (1993) Corticocortical connections of area F3 (SMA-proper) and area F6 (pre-SMA) in the macaque monkey. *J. Comp. Neurol.*, **338**, 114–140.
Matsuzaka, Y., Aizawa, H. & Tanji, J. (1992) A motor area rostral to the supplementary motor area (presupplementary motor area) in the monkey: neuronal activity during a learned motor task. *J. Neurophysiol.*, **68**, 653–662.
Mendoza, G. & Merchant, H. (2014) Motor system evolution and the emergence of high cognitive functions. *Prog. Neurobiol.*, **122**, 73–93.
Merchant, H. & Georgopoulos, A.P. (2006) Neurophysiology of perceptual and motor aspects of interception. *J. Neurophysiol.*, **95**, 1–13.
Merchant, H. & Honing, H. (2014) Are non-human primates capable of rhythmic entrainment? Evidence for the gradual audiomotor evolution hypothesis. *Front. Neurosci.*, **7**, 274.
Merchant, H., Zainos, A., Hernández, A., Salinas, E. & Romo, R. (1997) Functional properties of primate putamen neurons during the categorization of tactile stimuli. *J. Neurophysiol.*, **77**, 1132–1154.
Merchant, H., Battaglia-Mayer, A. & Georgopoulos, A.P. (2001) Effects of optic flow in motor cortex and area 7a. *J. Neurophysiol.*, **86**, 1937–1954.
Merchant, H., Battaglia-Mayer, A. & Georgopoulos, A.P. (2003) Functional organization of parietal neuronal responses to optic-flow stimuli. *J. Neurophysiol.*, **90**, 675–682.
Merchant, H., Battaglia-Mayer, A. & Georgopoulos, A.P. (2004a) Neural responses in motor cortex and area 7a to real and apparent motion. *Exp. Brain Res.*, **154**, 291–307.
Merchant, H., Battaglia-Mayer, A. & Georgopoulos, A.P. (2004b) Neural responses during interception of real and apparent circularly moving stimuli in motor cortex and area 7a. *Cereb. Cortex*, **14**, 314–331.
Merchant, H., Fortes, A.F. & Georgopoulos, A.P. (2004c) Short-term memory effects on the representation of two-dimensional space in the rhesus monkey. *Anim. Cogn.*, **7**, 133–143.
Merchant, H., Zarco, W. & Prado, L. (2008a) Do we have a common mechanism for measuring time in the hundreds of millisecond range? Evidence from multiple-interval timing tasks. *J. Neurophysiol.*, **99**, 939–949.
Merchant, H., Zarco, W., Bartolo, R. & Prado, L. (2008b) The context of temporal processing is represented in the multidimensional relationships between timing tasks. *PLoS One*, **3**, e3169: 1–9.
Merchant, H., Zarco, W., Prado, L. & Pérez, O. (2009) Behavioral and neurophysiological aspects of target interception. *Adv. Exp. Med. Biol.*, **629**, 201–220.
Merchant, H., Crowe, D.A., Robertson, M.S., Fortes, A.F. & Georgopoulos, A.P. (2011a) Top-down spatial categorization signal from prefrontal to posterior parietal cortex in the primate. *Front. Syst. Neurosci.*, **5**, 69.
Merchant, H., Zarco, W., Pérez, O., Prado, L. & Bartolo, R. (2011b) Measuring time with different neural chronometers during a synchronization-continuation task. *Proc. Natl. Acad. Sci. USA*, **108**, 19784–19789.
Merchant, H., Harrington, D. & Meck, W.H. (2013a) Neural basis of the perception and estimation of time. *Annu. Rev. Neurosci.*, **36**, 313–336.
Merchant, H., Pérez, O., Zarco, W. & Gámez, J. (2013b) Interval tuning in the primate medial premotor cortex as a general timing mechanism. *J. Neurosci.*, **33**, 9082–9096.
Merchant, H., Crowe, D.A., Fortes, A.F. & Georgopoulos, A.P. (2014) Cognitive modulation of local and callosal neural interactions in decision making. *Front. Neurosci.*, **8**, 245.
Merchant, H., Grahn, J., Trainer, L., Rohrmeier, M. & Fitch, TW. (2015) Finding the beat, a neuro-computational approach. *Philos. T. Roy. Soc. B.*, **370**.
Nagasaka, Y., Chao, Z.C., Hasegawa, N., Notoya, T. & Fujii, N. (2013) Spontaneous synchronization of arm motion between Japanese macaques. *Sci. Rep.*, **3**, 1151.
Naselaris, T., Merchant, H., Amirikian, B. & Georgopoulos, A.P. (2005) Spatial reconstruction of trajectories of an array of recording microelectrodes. *J. Neurophysiol.*, **93**, 2318–2330.
Naselaris, T., Merchant, H., Amirikian, B. & Georgopoulos, A.P. (2006) Large-scale organization of preferred directions in the motor cortex. II. Analysis of local distributions. *J. Neurophysiol.*, **96**, 3237–3247.
Patel, A.D. (2014) The evolutionary biology of musical rhythm: was darwin wrong? *PLoS Biol.*, **12**, e1001821.
Perez, O., Kass, R. & Merchant, H. (2013) Trial time warping to discriminate stimulus-related from movement-related neural activity. *J. Neurosci. Meth.*, **212**, 203–210.

Phillips-Silver, J. & Trainor, L.J. (2005) Feeling the beat: movement influences infant rhythm perception. *Science*, **308**, 1430.
Rilling, J.K., Glasser, M.F., Preuss, T.M., Ma, X., Zhao, T., Hu, X. & Behrens, T.E.J. (2008) The evolution of the arcuate fasciculus revealed with comparative DTI. *Nature*, **11**, 426–428.
de la Rocha, J., Doiron, B., Shea-Brown, E., Josić, K. & Reyes, A. (2007) Correlation between neural spike trains increases with firing rate. *Nature*, **448**, 802–806.
Romo, R. & Schultz, W. (1987) Neuronal activity preceding self-initiated or externally timed arm movements in area 6 of monkey cortex. *Exp. Brain Res.*, **67**, 656–662.
Romo, R., Ruiz, S., Crespo, P., Zainos, A. & Merchant, H. (1993) Representation of tactile signals in primate supplementary motor area. *J. Neurophysiol.*, **70**, 2690–2694.
Romo, R., Merchant, H., Zainos, A. & Hernández, A. (1996) Categorization of somaestetic stimuli: sensorimotor performance and neuronal activity in primary somatic sensory cortex of awake monkeys. *NeuroReport*, **7**, 1273–1279.
Romo, R., Merchant, H., Zainos, A. & Hernández, A. (1997) Categorical perception of somesthetic stimuli: psychophysical measurements correlated with neuronal events in primate medial premotor cortex. *Cereb. Cortex*, **7**, 317–326.
Rorden, C., Karnath, H.O. & Bonilha, L. (2007) Improving lesion-symptom mapping. *J. Cognitive Neurosci.*, **19**, 1081–1088.
Stauffer, C.C., Haldemann, J., Troche, S.J. & Rammsayer, T.H. (2012) Auditory and visual temporal sensitivity: evidence for a hierarchical structure of modality-specific and modality-independent levels of temporal information processing. *Psychol. Res.*, **76**, 20–31.
Tanji, J. & Evarts, E.V. (1976) Anticipatory activity of motor cortex neurons in relation to direction of an intended movement. *J. Neurophysiol.*, **39**, 1062–1068.
Tanji, J. & Kurata, K. (1982) Comparison of movement-related activity in two cortical motor areas of primates. *J. Neurophysiol.*, **48**, 633–653.
Tanji, J. & Kurata, K. (1985) Contrasting neuronal activity in supplementary and precentral motor cortex of monkeys. I. Responses to instructions determining motor responses to forthcoming signals of different modalities. *J. Neurophysiol.*, **53**, 129–141.
Uhrig, L., Dehaene, S. & Jarraya, B. (2014) A hierarchy of responses to auditory regularities in the macaque brain. *J. Neurosci.*, **34**, 1127–1132.
Wing, A.M. (2002) Voluntary timing and brain function: an information processing approach. *Brain Cognition*, **48**, 7–30.
Wise, S.P. (1985) The primate premotor cortex: past, present, and preparatory. *Annu. Rev. Neurosci.*, **8**, 1–19.
Zar, J.H. (1999) *Biostatistical Analysis*. Prentice Hall, New Jersey.
Zarco, W., Merchant, H., Prado, L. & Mendez, J.C. (2009) Subsecond timing in primates: comparison of interval production between human subjects and rhesus monkeys. *J. Neurophysiol.*, **102**, 3191–3202.